# Search for $\tau \to 3\mu$ decay at the CMS experiment in Run-II

Federica Maria Simone

PhD School in Physics - XXXIV Cycle - Second year report
November 2, 2020
Thesis advisors: dr. Anna Colaleo, dr. Omer J. Verwilligen

## 1 Introduction

In the Standard Model (SM), lepton flavour violation (LFV) involving charged leptons is allowed by neutrino oscillations; it can therefore occur only through loop processes which are stronghly suppressed and not accessible at present day experiments [1, 2]. Several extensions of the SM, however, allow for LFV in the charged sector with sizeable branching fractions. In particular, some models based on Supersimmetry (SUSY) have strongly enhanced rates for such decays ($\mathcal{O}(10^{-8})$) [3, 4]; this makes LFV an ideal playground to search for beyond the SM physics (BSM).
The neutrinoless decay of the tau lepton into three muons ($\tau \to 3\mu$) is a promising LFV decay channel for the LHC experiments, since it has a clear signature given by the three muons in the final state, it is strongly enhanced by BSM theories since they typically couple through the higher mass particles and it is feasible at pp colliders given the high number of tau leptons produced.
The more relevant source of $\tau$ leptons at the LHC are decays of c- and b-hadrons, dominated by the $D_s \to \tau\nu$, $B \to \tau\nu$ and referred as heavy flavour channel (HF), followed by $W \to \tau\nu$ and $Z \to \tau\tau$ decays. Despite $\tau$ produced in the HF channel are the most abundant, they are significantly boosted in the forward direction thus being more difficult to reconstruct because of the higher background.

## 2 State of the art

The search for this decay has already been carried out by several experiments and no evidence has been observed so far. The stricter limit on the branching fraction has been set by the Belle collaboration with $\mathcal{B}(\tau \to 3\mu) < 2.1 \cdot 10^{-8}$ at 90% confidence level [5]. This search in the HF and W channels has been performed at the CMS experiment using pp collision data collected at $\sqrt{s} = 13\,\text{TeV}$ in 2016, corresponding to an integrated luminosity of 33 fb$^{-1}$. The upper limit on the branching fraction set by the combined HF+W analysis of 2016 data is $\mathcal{B}(\tau \to 3\mu) < 8.0 \cdot 10^{-8}$ at 90% confidence level [6].
Extending the search for the $\tau \to 3\mu$ decay to the full Run II data taking corresponding to $\sim 120$ fb$^{-1}$ would exploit an increased statistics thus possibly providing a stricter upper limit on the branching fraction. This PhD research aims to analyse the full Run II data (i.e. including data collected in 2017 and 2018) using $\tau$ leptons from B and D decays to search for the $\tau \to 3\mu$ decay.

## 3 Report on progress: analysis of data collected by CMS in 2017 and 2018

### 3.1 Datasets and simulated samples

The analysis is based on pp collision data at a center-of-mass energy of 13 TeV collected during the Run-II of LHC with the CMS detector. As this search has been already performed on data collected in 2016, we will focus on 2017 and 2018 datasets corresponding to a total integrated luminosity of $\mathcal{L} = 97.7$ fb$^{-1}$. The collision data sets, run ranges, and integrated luminosity per data set, are listed in Table 1 and 2 . The

| 2017 Datasets | Run range | Integrated luminosity ($fb^{-1}$) |
|---|---|---|
| /DoubleMuonLowMass/Run2017B-31Mar2018-v1/MINIAOD | 297046-299329 | 4.79 |
| /DoubleMuonLowMass/Run2017C-31Mar2018-v1/MINIAOD | 299368-302029 | 9.63 |
| /DoubleMuonLowMass/Run2017D-31Mar2018-v1/MINIAOD | 302030-303434 | 4.24 |
| /DoubleMuonLowMass/Run2017E-31Mar2018-v1/MINIAOD | 303824-304797 | 9.30 |
| /DoubleMuonLowMass/Run2017F-31Mar2018-v1/MINIAOD | 305040-306462 | 10.04 |
| **Total** | **297046-306462** | **38.00** |

Table 1

| 2018 Datasets | Run range | Integrated luminosity ($fb^{-1}$) |
|---|---|---|
| /DoubleMuonLowMass/Run2018A-17Sep2018-v1/MINIAOD | 315252 - 316995 | 13.98 |
| /DoubleMuonLowMass/Run2018B-17Sep2018-v1/MINIAOD | 316998 - 319312 | 7.06 |
| /DoubleMuonLowMass/Run2018C-17Sep2018-v1/MINIAOD | 319313 - 320393 | 6.90 |
| /DoubleMuonLowMass/Run2018D-PromptReco-v2/MINIAOD | 320394 - 325273 | 31.75 |
| **Total** | **315252-325273** | **59.70** |

Table 2

data collected during the two years cannot be treated as a unique sample because changes in the High Level Trigger (HLT) used for the online selection of the events occurred between the two years.

Monte Carlo (MC) simulated samples are used to model the $\tau \to 3\mu$ decay in the more relevant $\tau$ production channels, namely the $D_s \to \tau\nu_\tau$, $B^\pm \to \tau\nu_\tau$ and $B^0 \to D^{-(*)}\tau^+\nu_\tau$. The events are generated with PYTHIA. The full simulation and reconstruction reproducing the 2017 and 2018 data taking conditions is then performed for the events containing at least 2 generated muons with $p_T > 2.7$ GeV and $|\eta| < 2.4$. These requirements match the CMS detector acceptance for muon reconstruction while being looser than the requirement at HLT level.

The $D_s \to \phi(\mu\mu)\pi$ decay is used to measure signal event rate associated with hadronically produced $\tau$-leptons. Moreover, this decay is used to compare data with MC simulation to evaluate systematic uncertainties on the final signal yields and to monitor the data taking stability. For this reason a MC sample for the $D_s \to \phi(\mu\mu)\pi$ decay is generated with similar settings as the signal samples.

## 3.2 Trigger

The High Level Trigger (HLT) used for the online selection of the events in 2017 (2018) requires 2 muons with $p_T > 3.0$ GeV and one additional track (tracker muon) with $p_T > 1.2$ GeV in the final state. The invariant mass of the three objects is required to be within 1.60 and 2.02 GeV and their common vertex is displaced from the beam-spot by more than two sigmas. The requirement on the third muon implemented in the 2018 HLT makes it not compatible with the $D_s \to \phi(\mu\mu)\pi$ search which requires a pion track. Nevertheless, the 2017 HLT was scaled during 2018 by a factor 20 -meaning that it collected approximately 1/20 of the events- and it has been used to perform the analysis of the control channel on 2018 data.

## 3.3 Event selection

The events are required to have fired the HLT and at least one of its related L1 seeds. For the $\tau \to 3\mu$ search, events containing 3 reconstructed muons having $p_T > 2$ GeV and $|\eta| < 2.4$ which released at least 1 hit in the inner tracker and having total electric charge of $\pm 1$ are selected. The three $\mu$ tracks are fitted to a common vertex through a kinematic fit and these tracks are removed for the primary vertex position re-computation. The thus formed $3\mu$ candidate is then required to pass additional selections on the vertex quality, event topology, trigger matching.

Each muon must pass the particle flow (PF) reconstruction [7] within the CMS acceptance ($p_T > 2$ GeV and $|\eta| < 2.4$). The two muons with higher $p_T$ $\mu_1$ and $\mu_2$ are required to be reconstructed as global muons, while two exclusive categories of events are created based on the reconstruction of $\mu_3$:

1. $\mu_3$ is reconstructed as a global muon,
2. $\mu_3$ is not a global muon, but is reconstructed as a tracker muon.

The invariant mass if the $3\mu$ system is required to be within 1.62 and 2.0 GeV. A requirement on the collimation of pair of muon is applied cutting on $\Delta R < 0.8$ and $\Delta z < 0.5$ and for those pairs having opposite electric charge a veto on the $2\mu$ invariant mass is implemented in order to exclude the $\phi$ and $\omega$ meson resonances. Each of the muons should match one leg of the HLT object within $\Delta R < 0.03$ and $\Delta p_T/p_T < 0.1$. Finally if more than one $\tau$ candidate per event passes the selections, the one with best value of the $3\mu$ common vertex $\chi^2$ is kept.

### 3.4 Event categorization

In order to improve the search sensitivity, the events are split into three exclusive categories based on the relative resolution of the three-muons system invariant mass ($\rho$), computed propagating the resolution on the muon transverse momenta to the invariant mass computation. The categories are defined as A: $\rho < 0.007$, B: $\rho \in [0.007, 0.0105]$, C: $\rho > 0.0105$ and they relates to the pseudorapidity of the most forward muon, approximately corresponding to the central, overlap and endcap sectors of the CMS muon system [8].

As discussed in Section 3.3, two exclusive categories of events arise from the event selections based on the reconstruction of the lowest-$p_T$ muon. Those two categories are named "3global" and "2global1tracker" and for each category the events are further split in three subsets based on the value of $\rho$. The analysis is thus performed in 6 independent categories of events.

### 3.5 $D_s$ yield evaluation and Data-MC comparison

The $D_s \to \phi(\mu\mu)\pi$ analysis is performed using similar selections as used for the signal search. In this case, two reconstructed muons are required to have opposite charge, while loose requirements are applied to the additional track (i.e. the pion candidate). The invariant mass of the $2\mu$+1track system, showed in Fig. 1, is fitted using a falling exponential function for the background and two crystall-ball functions to model the $D^+$ and $D_s$ peaks. The $D_s$ production yield in data is extracted from the fit.

The $D_s$ yield is measured for each of the 2017 eras separately and compared with the prediction from the Monte Carlo simulation based on the integrated luminosity and on the $D_s \to \phi(\mu\mu)\pi$ decay branching fraction. The results are showed in Fig. 2a. This study allows us to spot anomalies in the 2017 eras B and F data taking, both related to hardware issues. In fact, at the beginning of 2017 the tracker detector was affected by a calibration problem which caused a drop in the track reconstruction efficiency for tracks in $1 < |\eta| < 1.5$, while in the middle of 2017 era F the DC/DC converters powering the pixel layers experienced a failure which caused the malfunctioning of a big fraction of the detector.

The data taking during 2018 was stable and this reflects in the $D_s$ measurement performed using the same HLT as 2017 which was prescaled by a factor 20 in 2018. The ratio between the $D_s$ production yield measured in 2018 and the value expected from simulation is reported in Fig. 2b.

For the full data taking period, the deficit in the $D_s$ yield production with respect to expectations is computed (red line in Fig. 2) and it is used as scale factor in the $D_s \to \tau \to 3\mu$ signal normalisation.

The $D_s \to \phi(\mu\mu)\pi$ channel is also used to compare distributions of relevant variables in both data and Monte Carlo. The distributions in MC are scaled by a factor $f_{MC}$ given by:

$$f_{MC} = \frac{\mathcal{L} \cdot \sigma(pp \to D_s) \cdot \mathcal{B}(D_s \to \phi(\mu\mu)\pi)}{N_{MC}} \tag{1}$$

Since the $D_s \to \phi(\mu\mu)\pi$ MC sample only contains decay events, the background contribution is subtracted from data exploiting the fitting procedure showed in Fig. 1. Distributions of relevant variables used in the analysis are compared in data and MC and they are shown in Fig. 3. A full description of the variables will be provided in Section 3.7.

### 3.6 MVA Muon Identification for global muons

As this analysis deals with low $p_T$ and high pseudorapidity muons, an important contribution to background comes from pions and ka0ns mis-reconstructed as muons. Dedicated studies performed on "Minimum Bias" MC samples have shown that the background events passing the analysis selections often include one fake muon in the final state. A custom MVA muon identification algorithm has been developed in the context

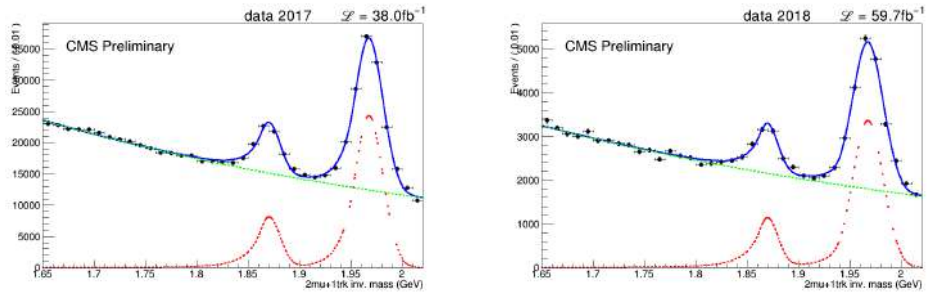


(a) (b)

Figure 1: Invariant mass of the two muons + 1 track system measured in the 2017 (left) and 2018 (right). The $D_s$ and $D^+$ peaks are fitted with Crystall Ball functions (red line), while the background is fitted with an exponential (green line). The combination of the two fits (blue line) is used to model the data (black dots).

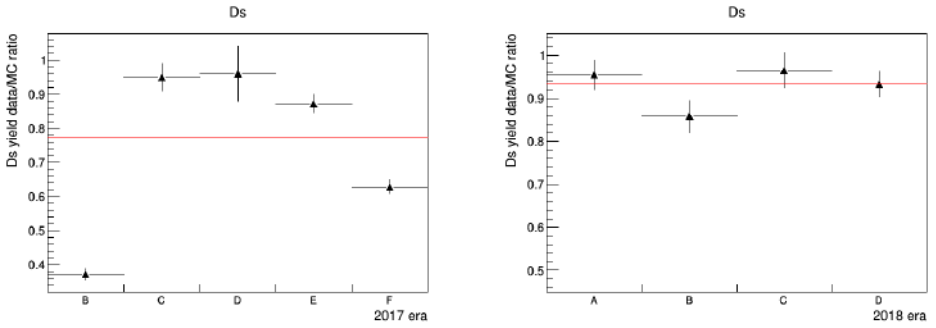


(a) (b)

Figure 2: Fitted $D_s \to \phi(\mu\mu)\pi$ yields for each of the 2017 (left) and 2018 (right) eras compared with expected number from simulation.

of the search for $B^0 \to \mu\mu$ decays at CMS [9] targeting misidentified muons and the output of such a discriminator is centrally available in the CMS software. Despite the good performances, this centrally available muon ID named "SoftMVA" doesn't match the requirements of this search as it was trained for muons having $p_T > 4$GeV and $|\eta| < 1.4$, while 30% of simulated $D_s \to \tau \to \mu\mu\mu$ events have at least one muon below the 4 GeV threshold.

A custom MVA Muon Identification algorithm has been then developed specifically for this analysis, in the light of the studies performed for the SoftMVA development. The main idea is to train a Boosted Decision Tree (BDT) using variables related to the quality of muon reconstruction, making use of simulated pions and kaons from D and B decays as background, while the lowest $p_T$ muons in the final state of $D_s \to \tau \to \mu\mu\mu$ MC is used as signal. All the MC samples used are reconstructed in realistic 2017 and 2018 conditions and the algorithm has been developed separately for the two years.

### 3.6.1 MC samples and event selection

In order to implement a discriminator for pions and kaons misidentified as global muons in the phase-space of interest for the $D/B \to \tau \to 3\mu$ search, simulated $\pi$ and K from D and B decays are used as background. The full list of processes and MC samples with pions and kaons in the final state used as background is reported in Table 3. The final state muons from the $D_s \to \tau \to 3\mu$ MC signal sample are used as signal.

For background, all samples are analysed asking for at least one muon reconstructed as global muon within the CMS acceptance per event. The muon is required to have valid simulation information about the generated particle matching with his track. Since a pion or kaon track can be reconstructed as a muon,

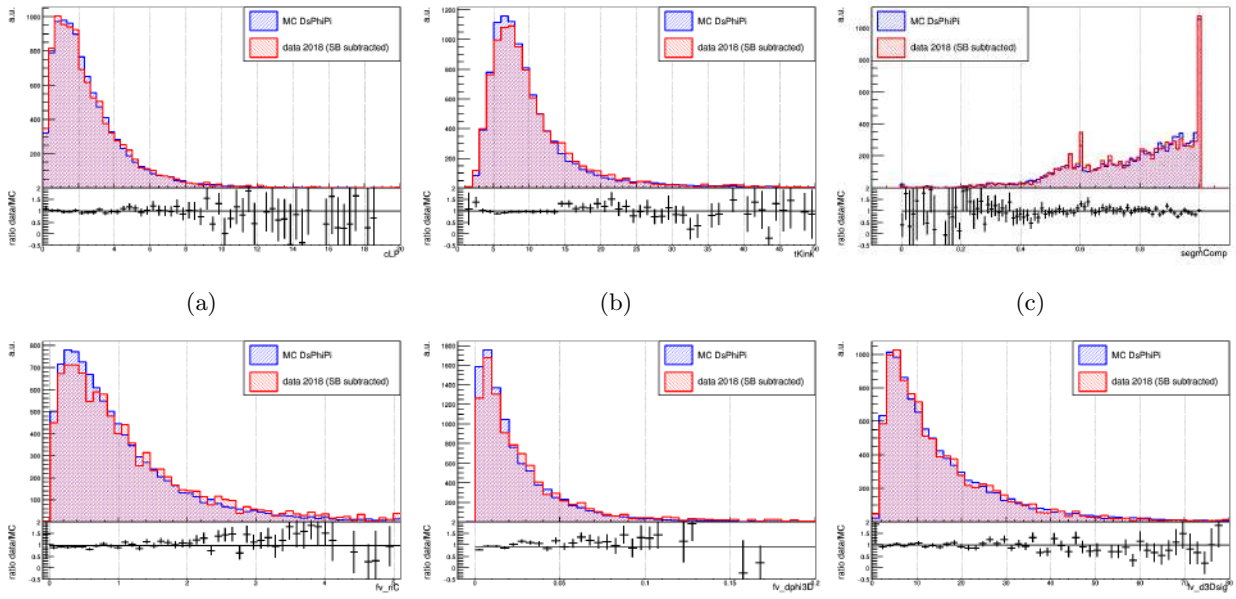


(a) (b) (c)

(d) (e) (f)

Figure 3: Distributions for some of the observables used in the BDT training in the $D_s \to \phi(\mu\mu)\pi$ MC (blue) and 2018 data (sideband subtracted, red).

| Process | Dataset name |
|---|---|
| $B_s^0 \to \pi^+\pi^-$ | /BsToPiPi_BMuonFilter_SoftQCDnonD_TuneCP5_13TeV-pythia8-evtgen/ |
| $B_s^0 \to K^+K^-$ | /BsToKK_SoftQCDnonD_TuneCP5_13TeV-pythia8-evtgen/ |
| $B_s^0 \to K^+K^-$ | /BsToKK_BMuonFilter_SoftQCDnonD_TuneCP5_13TeV-pythia8-evtgen/ |
| $B_d^0 \to K^+\pi^-$ or $K^0\pi^0$ | /BdToKPi_SoftQCDnonD_TuneCP5_13TeV-pythia8-evtgen/ |
| $B_d^0 \to K^+\pi^-$ or $K^0\pi^0$ | /BdToKPi_BMuonFilter_SoftQCDnonD_TuneCP5_13TeV-pythia8-evtgen/ |
| $B_d^0 \to K^+K^-$ or $K^0\bar{K}^0$ | /BdToKK_BMuonFilter_SoftQCDnonD_TuneCP5_13TeV-pythia8-evtgen/ |
| $B_d^0 \to \pi^+\pi^-$ or $\pi^0\pi^0$ | /BdToPiPi_BMuonFilter_SoftQCDnonD_TuneCP5_13TeV-pythia8-evtgen/ |
| **Year** | **Simulated conditions** |
| 2017 | RunIIFall17MiniAODv2-PU2017_12Apr2018_N1_94X_mc2017_realistic_v14-v1 |
| 2018 | RunIIAutumn18DRPremix-102X_upgrade2018_realistic_v15-v2 |

Table 3

this information allow us to separate muons from fakes. Muons matching at generator level with pions and kaons, together with muons coming from pions and kaons decaying in flight are used to build the background sample.

Signal muons are taken as the set of trailing muons $\mu_3$ in the $D_s \to \tau \to 3\mu$ events. The muon is required to be reconstructed as a global muon within the CMS acceptance and to match at generator level with a muon coming from tau decay. Moreover, the event must fire the HLT as asked in the $\tau \to 3\mu$ main analysis.

The phase space ($|\eta|$, $p_T$) covered by pions and kaons faking muons in the background samples does not match completely with the phase space of signal muons, as it can be seen in Fig. 4a and 5a showing the $p_T$ distributions for background and signal muons in barrel and endcap, respectively. For this reason, a reweighing procedure is applied to background muons. The ($|\eta|$, $p_T$) plane is segmented and the ratio between the 2-dimentional $|\eta|$, $p_T$ distributions of signal and background muons is computed. The value of the ratio for each 2-D bin is used as weight to be applied to the background samples. The resulting $p_T$ distributions are showed in Fig. 4b and 5b, again distinguishing between barrel and endcap.

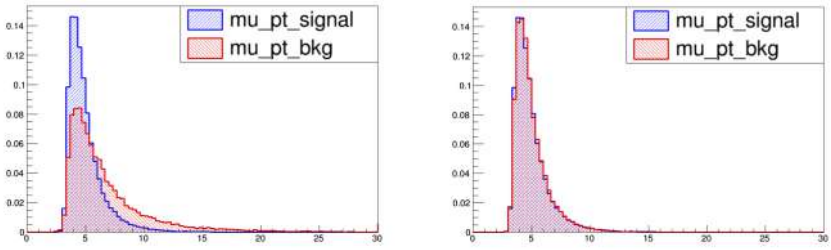


(a) (b)

Figure 4: Distribution of the transverse momenta of the muons used as background and signal for the training of the MVA muon ID, in the barrel ($|\eta| < 1.2$), before (a) and after (b) reweighing the phase space of the background muons.

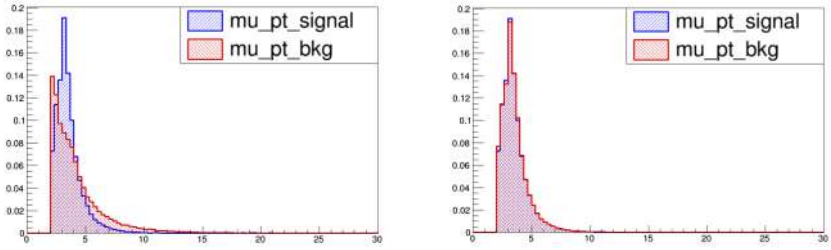


(a) (b)

Figure 5: Distribution of the transverse momenta of the muons used as background and signal for the training of the MVA muon ID, in the endcap ($|\eta| > 1.2$), before (a) and after (b) reweighing the phase space of the background muons.

### 3.6.2 BDT training for MVA Muon Identification

A Boosted Decision Tree (BDT) as implemented in the TMVA package of ROOT is trained separately for barrel and endcap using the signal and background samples described above, making use of a list of variables related to the quality of the muon track reconstruction, the kink of the track, the number of detectors tin the CMS muon system traversed by the muon and the matching between the muon track reconstructed in the muon system and the track in the tracker.

The initial list of available variables has been pruned performing a BDT optimisation procedure. As a first approach, all available variables (22 in total) were fed to the BDT. Based on variable ranking returned by the TMVA tool, the 7 variable with the highest importance common for barrel and endcap were identified as "core" variables. Among the remaining variables, the correlations between them were studied and coupled of strongly correlated variables (Pearson coefficient $> 0.7$) were selected. For each couple, the variable with the highest ranking was kept. Finally, after fixing the number of total variables, all the remaining combinations were tested and the set providing the highest Receiver Operating Characteristic (ROC) integral was used.

A similar procedure based on maximising the area under the ROC curve has been used to tune the BDT settings in the TMVA tool. The final lists of 18 input variables and the BDT settings used are reported below, while the signal and background distributions for some of the input variables with higher discriminating power are shown in Fig. 6.

- **mu_combinedQuality_chi2LocalPosition**: A scalar resulting from the matrix-vector product $v^T M v$, where v corresponds to the difference in position of the Trajectory State On Surface (TSOS) of the standalone muon and the tracker track at the common surface and M corresponds to the related error matrix.
- **mu_combinedQuality_trkKink**: The kink algorithm applied to the global muon's inner track (log used).
- **mu_combinedQuality_glbTrackProbability**: The probability of the $\chi^2$ associated to the global track being larger than the one observed.

- **mu_Numberofvalidtrackerhits**: The amount of valid hits in the tracker.
- **mu_Numberofvalidpixelhits**: The amount of valid hits in the pixel detector.
- **mu_innerTrack_validFraction**: The number of valid hits of the inner track divided by the total number of hits and missing hits of the inner track.
- **mu_combinedQuality_chi2LocalMomentum**: see "mu_combinedQuality_chi2LocalPosition", replacing position with momentum.
- **mu_combinedQuality_staRelChi2**: The sum of $\chi^2$ estimates of the hits in the muon system with respect to the global muon track.
- **mu_combinedQuality_trkRelChi2**: The sum of $\chi^2$ estimates of the hits in the tracker with respect to the global muon track.
- **mu_combinedQuality_globalDeltaEtaPhi**: The squared difference in $\eta$ and $\phi$ of the standalone muon track and the tracker track on the common surface during track matching.
- **mu_combinedQuality_glbKink**: The kink algorithm applied on the global track (log used).
- **mu_trackerLayersWithMeasurement**: The amount of tracker layers with hits.
- **mu_validMuonHitComb**: The number of valid hits in the muon chambers computed combining RPC, DT and DCS hits.
- **mu_numberOfMatchedStations**: The number of muon stations containing matched segments.
- **mu_segmentCompatibility**: A measure of the track's compatibility with the muon hypothesis.
- **mu_timeAtIpInOutErr**: The uncertainty in the time of arrival at the interaction point for muons moving inside-out assuming $\beta = 1$.
- **mu_GLnormChi2**: The $\chi^2$ of the global muon track divided by the number of degrees of freedom of the fit.
- **mu_innerTrack_normalizedChi2**: The $\chi^2$ of the inner muon track divided by the number of degrees of freedom of the fit.
- **mu_outerTrack_normalizedChi2**: The $\chi^2$ of the outer muon track divided by the number of degrees of freedom of the fit.

### BDT settings:

- NTrees=1000, MinNodeSize=1.5%, MaxDepth=8
- BoostType=RealAdaBoost, AdaBoostBeta=0.3, UseBaggedBoost, BaggedSampleFraction=0.05
- SeparationType=GiniIndex, nCuts=-1 (automatically optimised by TMVA tool)
- Training/test splitting: Random. Fraction: 70/30

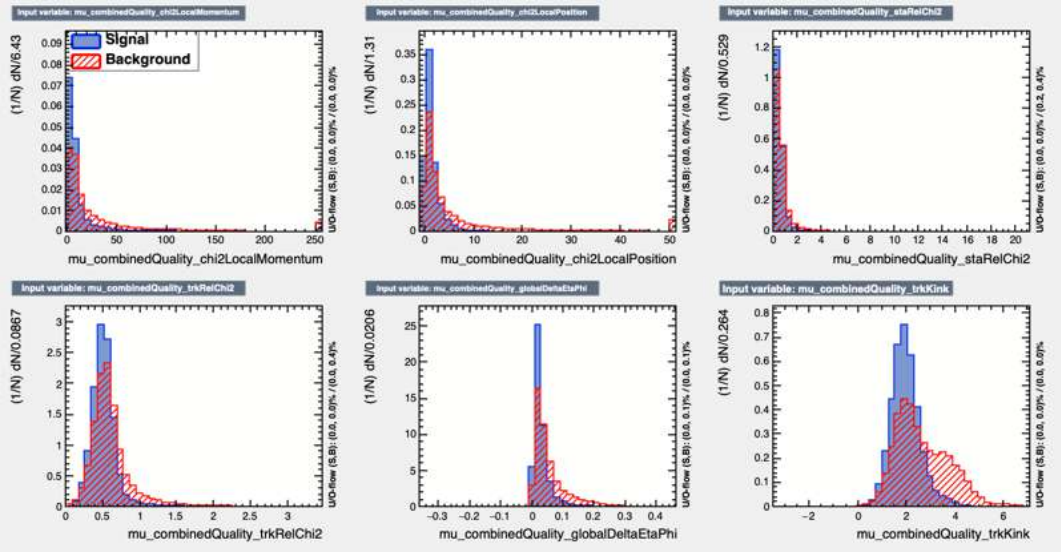


Figure 6: Signal and background distributions for some of the variables used to train the MVA Muon ID for global muons for $|\eta| > 1.2$ (endcap).

The BDT score evaluated on the training and test subsamples is reported in Fig. 7. The good discrimination power provided on pions and kaons misidentified as muons makes this BDT output a good indicator for the muon reconstruction quality. Moreover, it carries information from all aspects of the CMS muon reconstruction algorithm as well as all subdetectors involved.

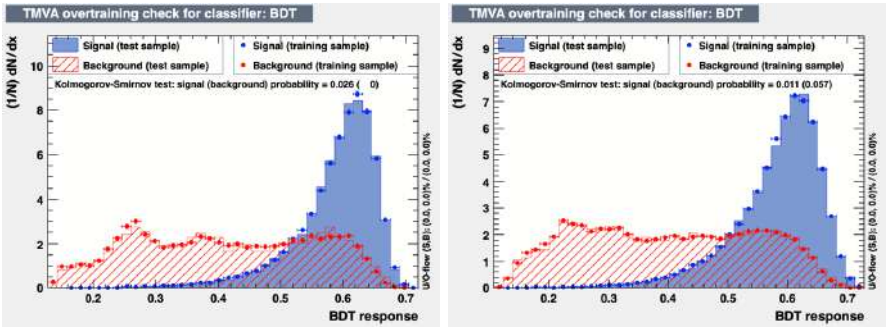


(a) (b)

Figure 7: MVA muon ID score distributions for signal and background as returned after training and test evaluation by the TMVA tool for muons in barrel (a) and endcap (b).

### 3.6.3 Performance of MVA Muon Identification for global muons

The MVA Muon Identification as been trained on muons from tau decay as signal and on pions and kaons misidentified as muons as background. In both cases, the muons passed the global reconstruction. The score of the BDT can be then used to qualify muons in data and MC in the $\tau \to 3\mu$ search in order to reject fake muons in data. The distribution of MVA muon ID score evaluated on data and signal samples is showed in Fig. 8. It can be seen that data and MC share a large fraction of "good" muons, as expected, but a tail at low BDT score in data indicates a contribution from $\pi$ and K.

A comparison between this newly implemented discriminator and the existing "SoftMVA" flag has been performed both looking at the shapes in data and MC in the $\tau \to 3\mu$ search, both comparing the ROC curves on signal (real muons) and background ($\pi$, K, $\mu$ from $\pi$ and K decays). In both cases, the new MVA Muon ID performs better than "SoftMVA", specially for muons with $p_T < 4GeV$.

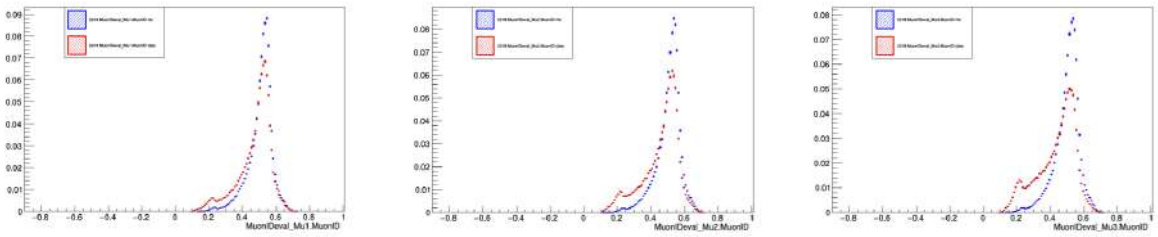

(a) (b) (c)

Figure 8: MVA muon ID score evaluated on data and $\tau \to 3\mu$ signal events passing analysis selections. The evaluation is performed for the final state muons $\mu_1$, $\mu_2$ and $\mu_3$ which are $p_T$ sorted.

## 3.7 Multi-variate analysis for background rejection

As discussed in Sections 3.3 and 3.4, the search for the $\tau \to 3\mu$ decays lead to 6 exclusive categories of data and signal events, 3 based on the $3\mu$ mass resolution (A, B, C) and 2 based on the reconstruction of the trailing muon (3global, 2global1tracker). For each of the thus formed categories, a Multi-Variate Analysis is implemented to reject the background. The algorithm chosen is again a BDT as implemented in the

| Name | Description | Event category |
|---|---|---|
| cLP | $\chi^2$ for the position matching between the muon inner track and the outer track (maximum of the three muons). | all |
| tKink | Kink algorithm applied to the muon inner track (max. of the three muons). | all |
| segmComp | Value of the position compatibility between the inner track and muon segment (minimum of the three muons). | all |
| fv_nC | Normalized $\chi^2$ for the $3\mu$ vertex. | all |
| fv_dphi3D | Angle between the $3\mu$ momentum vector and the PV-SV vector. | all |
| fv_d3Dsig | Significance of the 3D displacement of the $3\mu$ vertex with respect to the primary vertex (PV). | all |
| d0sig | Minimum significance of the transverse I.P. of the $\mu$ track with respect to the PV. | all |
| mindca_iso | Minimum of the distance of closest approach to the $3\mu$ vertex to any other track in the event having $p_T > 1$ GeV. | all |
| trkRel | Ratio of the $p_T$ surrounding ($\Delta R < 0.3$, dca $<$ 1mm) tracks to that of the muon (maximum of the three muons). | all |
| MVA mu ID (global) | Score of the MVA muon discriminator implemented for global muons (see Section 3.6.2). The values for all three muons are used. | 3global |
| MVA mu ID (tracker) | Score of an additional MVA muon discriminator implemented for tracker muons (not documented here). The value for the trailing muon is used. | 2global1tracker |
| Pt_tripl | Transverse momentum of the $\tau$ candidate. | 3global |
| abs(dxy3/dxyErr3) | Significance of the transverse I.P. for $\mu_3$ with respect to the PV. | 3global (A, B) |
| Pmu3 | Momentum of the trailing muon of the triplet. | 2global1tracker |
| minMatchedStations | Minimum number of matched stations in the muon system. | 2global1tracker |

Table 4

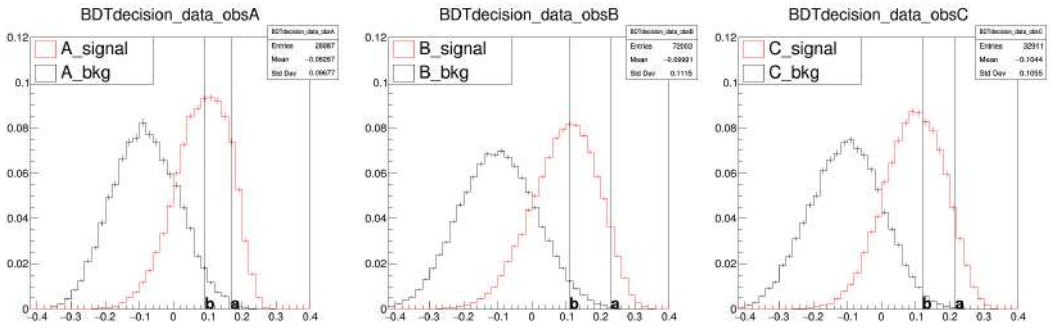


(a) (b) (c)

Figure 9: BDT response for the three categories of events, in the 3global case for 2018 data and MC. The 2 vertical bars indicate the cuts for sub-categories definition.

TMVA toolkit. The BDT is trained using MC events as signal, data from the $3\mu$ invariant mass region $[1.65, 1.73] \cup [1.82, 1.90]$ GeV (referred as sidebands - SB) as background. For each category, 80% of the events is used for training, while the remaining 20% is used for testing purposes.

The set of input variables given to the BDT is implemented differently for each category. Moreover, different implementations have been tested for 2017 and 2018 data as they show different features related to the data taking conditions and to the HLT used. The list of the variables is summarised in Table 4, together with a short description of the observables and the category of event in which they were used.

The BDT is trained separately in each event category and separately for 2017 and 2018 data and MC samples. As an example, the BDT score distributions on signal and data for categories "3global" A, B, C for 2018 are showed in Fig. 9. The vertical lines on the plots indicate the additional categorisation done for background rejection so that the combined signal significance in the best two categories is maximised, while the worst one is discarded. The categories resulting based on the BDT score are numbered 1 and 2, with the number 1 being the most background-free.

| category/year | 3global | 2global1tracker |
|---|---|---|
| 2017 | $\mathcal{B}(\tau \to 3\mu) = 0.71 \times 10^{-7}$ | $\mathcal{B}(\tau \to 3\mu) = 1.66 \times 10^{-7}$ |
| 2018 | $\mathcal{B}(\tau \to 3\mu) = 0.46 \times 10^{-7}$ | $\mathcal{B}(\tau \to 3\mu) = 1.47 \times 10^{-7}$ |

Table 5: Expected upper limit on the $tau \to 3\mu$ branching ratio at 90% confidence level.

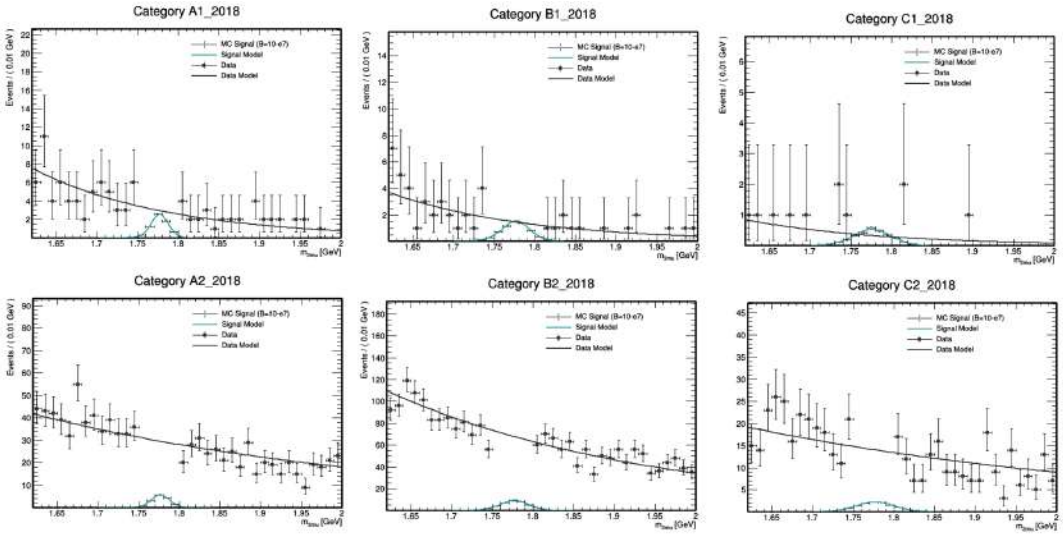


Figure 10: $3\mu$ mass distributions in the six independent event categories as defined in the text, for the 3global case in 2018. Data are shown with points and the signal region is blinded. The background-only fit and the expected signal for $B(\tau \to 3\mu) = 10^{-7}$ are shown. with lines.

### 3.8 Preliminary results

The signal yields in each of the event categories is obtained by normalising the number of events for each production mode to the related cross section. The signal yield is then corrected for the discrepancy in the number of $D_s$ observed in data and MC. Finally, the $3\mu$ mass spectra are parameterised with a fitting procedure for both signal (gaussian + crystal ball function) and background (falling exponential). As an example, the $3\mu$ mass distributions in the six event categories for the 3global case in 2018 datasets are shown in Fig. 10.

The CMS Higgs Combined Limit tool is used to perform statistical analysis. Upper limits on branching fraction $\tau \to 3\mu$ are set using the modified frequentist CLs criterion. The chosen test statistic used to determine how signal or background-like the data are, is based on the profile likelihood ratio. Systematic uncertainties are incorporated in the analysis via nuisance parameters and are treated according to the frequentist paradigm. The fit is implemented separately for each event category and the expected upper limit is then obtained combining the yields. The expected upper limit for the 3global and 2global1tracker categories obtained analysing the 2017 and 2018 data are reported in Table 5.

The combined expected upper limit at 90% C.L. is:

$$\mathcal{B}(\tau \to 3\mu) = 0.35 \times 10^{-7} \text{at } 90\% \text{C.L.} \tag{2}$$

## 4 Conclusions and plans

The analysis workflow as been fully implemented on 2017 and 2018 datasets thus exploiting the full Run-II statistics if combined with the 2016 published result. A custom MVA muon discriminator has been implemented for pions and kaons mis-reconstructed as global muons. Moreover, the per-event BDT for the background rejection has been optimised and new variables have been added. An exclusive category

of events based on the reconstruction of the lowest-$p_T$ muon has been implemented to further improve the search sensitivity.

Most of the systematic uncertainties have been evaluated and the results are not discussed in this report for brevity. The evaluation of the uncertainty on the BDT response using the $D_s \to \phi(\mu\mu)\pi$ control channel is in progress. Dedicated background studies not discussed in this document are ongoing. An optimisation of the vetos applied to the $2\mu$ mass to reject contribution of $\phi$ and $\omega$ mesons is also in progress. In this iteration the per-event BDT has been trained separately for the two years. Assessing the BDT performance in case of a unique training is among the next steps of this analysis.

The final result of the $\tau \to 3\mu$ in the HF channel on 2017 and 2018 data will be then combined with the W channel. Aside optimisations of the background rejection and fine-tuning of the BDT, the plan is to finalise the analysis workflow and compute the missing systematic uncertainties by the end of 2020 targeting the winter conferences in 2021.

# 5 Schools and workshops

- ISOTDAQ - International School of Trigger and Data Acquisition, University of Valencia, Spain, 13-22 January 2020.

# 6 Conference talks and posters

- "Recent CMS heavy flavour physics results", $9^{th}$ International Conference on New Frontiers in Physics, Creta, Greece, Sept 4 - Oct 2 2020 (virtual).

# 7 Research abroad

- **Special INFN Associate Programme in the Framework of the LHC at CERN**
  Contract as Cooperation Associate: Jan 2020 – Jan 2021
  Project: "Search for $\tau \to 3\mu$ decay at the CMS experiment using full Run-II data and preparation for Run-III"

# References


[1] Hernández-Tomé, G., López Castro, G. and Roig, P. *Flavor violating leptonic decays of $\tau$ and $\mu$ leptons in the Standard Model with massive neutrinos*. Eur. Phys. J. C 79, 84 (2019) https://doi.org/10.1140/epjc/s10052-019-6563-4

[2] A. Soffer. *B-meson decays into final states with a $\tau$ lepton*. Modern Physics Letters A 29.07 (2014): 1430007. doi: 10.1142/s0217732314300079. arXiv:1401.7947

[3] K.S. Babu and C. Kolda. *Higgs-Mediated $\tau \to \mu\mu\mu$ in the Supersymmetric See-saw Model*. Phys. Rev. Lett., 89 (2002), 241802, doi:10.1103/PhysRevLett.89.241802, arXiv:hep-ph/0206310v2.

[4] R. Barbier et al. *R-parity violating supersymmetry*. Physics Reports, 420 (2005), 1, doi:10.1016/j.physrep.2005.08.006, arXiv:hep-ph/0406039.

[5] Belle Collaboration. *Search for Lepton Flavor Violating Tau Decays into Three Leptons with 719 Million Produced Tau+Tau- Pairs*. Phys. Lett. B 687 (2010) 139, doi:10.1016/j.physletb.2010.03.037, arXiv:1001.3221.

[6] CMS Collaboration. *Search for the lepton flavor violating decay $\tau \to 3\mu$ in proton-proton collisions at sqrt(s) = 13TeV*. CMS-PAS-BPH-17-004, http://cds.cern.ch/record/2668282?ln=en.

[7] CMS Collaboration. *Particle-flow reconstruction and global event description with the CMS detector*. JINST 12 (2017) P10003, arXiv:1706.04965.

[8] CMS Collaboration. *Performance of the CMS muon detector and muon reconstruction with proton-proton collisions at sqrt(s) = 13TeV*. JINST 13 (2018) P06015, arXiv:1804.04528.

[9] CMS Collaboration. *Measurement of properties of $B_s^0 \to \mu^+\mu^-$ decays and search for $B^0 \to \mu^+\mu^-$ with the CMS experiment*. HEP 04 (2020) 188, arXiv:1910.12127.

# 8 Publications


1. A. M. Sirunyan *et al.* [CMS], "Search for supersymmetry in proton-proton collisions at $\sqrt{s} = 13$ TeV in events with high-momentum Z bosons and missing transverse momentum," JHEP **09** (2020), 149 doi:10.1007/JHEP09(2020)149 [arXiv:2008.04422 [hep-ex]].

2. A. M. Sirunyan *et al.* [CMS], "Reconstruction of signal amplitudes in the CMS electromagnetic calorimeter in the presence of overlapping proton-proton interactions," JINST **15** (2020) no.10, P10002 doi:10.1088/1748-0221/15/10/P10002 [arXiv:2006.14359 [physics.ins-det]].

3. A. M. Sirunyan *et al.* [CMS], "Observation of the Production of Three Massive Gauge Bosons at $\sqrt{s}$ =13 TeV," Phys. Rev. Lett. **125** (2020) no.15, 151802 doi:10.1103/PhysRevLett.125.151802 [arXiv:2006.11191 [hep-ex]].

4. A. M. Sirunyan *et al.* [CMS], "Performance of the CMS Level-1 trigger in proton-proton collisions at $\sqrt{s} = 13$ TeV," JINST **15** (2020) no.10, P10017 doi:10.1088/1748-0221/15/10/P10017 [arXiv:2006.10165 [hep-ex]].

5. A. M. Sirunyan *et al.* [CMS], "Search for resonant pair production of Higgs bosons in the $bbZZ$ channel in proton-proton collisions at $\sqrt{s} = 13$ TeV," Phys. Rev. D **102** (2020) no.3, 032003 doi:10.1103/PhysRevD.102.032003 [arXiv:2006.06391 [hep-ex]].

6. A. M. Sirunyan *et al.* [CMS], "Search for a light pseudoscalar Higgs boson in the boosted $\mu\mu\tau\tau$ final state in proton-proton collisions at $\sqrt{s} = 13$ TeV," JHEP **08** (2020), 139 doi:10.1007/JHEP08(2020)139 [arXiv:2005.08694 [hep-ex]].

7. A. M. Sirunyan *et al.* [CMS], "Search for a light charged Higgs boson in the $H^{\pm} \to cs$ channel in proton-proton collisions at $\sqrt{s} = 13$ TeV," Phys. Rev. D **102** (2020) no.7, 072001 doi:10.1103/PhysRevD.102.072001 [arXiv:2005.08900 [hep-ex]].

8. A. M. Sirunyan *et al.* [CMS], "Observation of the $B_s^0 \to X(3872)\phi$ decay," Phys. Rev. Lett. **125** (2020) no.15, 152001 doi:10.1103/PhysRevLett.125.152001 [arXiv:2005.04764 [hep-ex]].

9. G. Aad *et al.* [CMS and ATLAS], "Combination of the W boson polarization measurements in top quark decays using ATLAS and CMS data at $\sqrt{s} = 8$ TeV," JHEP **08** (2020) no.08, 051 doi:10.1007/JHEP08(2020)051 [arXiv:2005.03799 [hep-ex]].

10. A. M. Sirunyan *et al.* [CMS], "Measurements of production cross sections of WZ and same-sign WW boson pairs in association with two jets in proton-proton collisions at $\sqrt{s} = 13$ TeV," Phys. Lett. B **809** (2020), 135710 doi:10.1016/j.physletb.2020.135710 [arXiv:2005.01173 [hep-ex]].

11. A. M. Sirunyan *et al.* [CMS], "Measurement of CKM matrix elements in single top quark $t$-channel production in proton-proton collisions at $\sqrt{s} = 13$ TeV," Phys. Lett. B **808** (2020), 135609 doi:10.1016/j.physletb.2020.135609 [arXiv:2004.12181 [hep-ex]].

12. A. M. Sirunyan *et al.* [CMS], "Identification of heavy, energetic, hadronically decaying particles using machine-learning techniques," JINST **15** (2020) no.06, P06005 doi:10.1088/1748-0221/15/06/P06005 [arXiv:2004.08262 [hep-ex]].

13. A. M. Sirunyan *et al.* [CMS], "Search for disappearing tracks in proton-proton collisions at $\sqrt{s} = 13$ TeV," Phys. Lett. B **806** (2020), 135502 doi:10.1016/j.physletb.2020.135502 [arXiv:2004.05153 [hep-ex]].

14. A. M. Sirunyan *et al.* [CMS], "Measurement of quark- and gluon-like jet fractions using jet charge in PbPb and pp collisions at 5.02 TeV," JHEP **07** (2020), 115 doi:10.1007/JHEP07(2020)115 [arXiv:2004.00602 [hep-ex]].

15. A. M. Sirunyan *et al.* [CMS], "The production of isolated photons in PbPb and pp collisions at $\sqrt{s_{\mathrm{NN}}} = 5.02$ TeV," JHEP **07** (2020), 116 doi:10.1007/JHEP07(2020)116 [arXiv:2003.12797 [hep-ex]].

16. A. M. Sirunyan *et al.* [CMS], "Measurements of $\mathrm{t\bar{t}}H$ Production and the CP Structure of the Yukawa Interaction between the Higgs Boson and Top Quark in the Diphoton Decay Channel," Phys. Rev. Lett. **125** (2020) no.6, 061801 doi:10.1103/PhysRevLett.125.061801 [arXiv:2003.10866 [hep-ex]].

17. A. M. Sirunyan *et al.* [CMS], "Measurement of the cross section for $\mathrm{t\bar{t}}$ production with additional jets and b jets in pp collisions at $\sqrt{s} = 13$ TeV," JHEP **07** (2020), 125 doi:10.1007/JHEP07(2020)125 [arXiv:2003.06467 [hep-ex]].

18. A. M. Sirunyan *et al.* [CMS], "Pileup mitigation at CMS in 13 TeV data," JINST **15** (2020) no.09, P09018 doi:10.1088/1748-0221/15/09/P09018 [arXiv:2003.00503 [hep-ex]].

19. A. M. Sirunyan *et al.* [CMS], "Measurement of the cross section for electroweak production of a Z boson, a photon and two jets in proton-proton collisions at $\sqrt{s}$ = 13 TeV and constraints on anomalous quartic couplings," JHEP **06** (2020), 076 doi:10.1007/JHEP06(2020)076 [arXiv:2002.09902 [hep-ex]].

20. A. M. Sirunyan *et al.* [CMS], "Measurement of the $\Upsilon$(1S) pair production cross section and search for resonances decaying to $\Upsilon$(1S)$\mu^+\mu^-$ in proton-proton collisions at $\sqrt{s}$ = 13 TeV," Phys. Lett. B **808** (2020), 135578 doi:10.1016/j.physletb.2020.135578 [arXiv:2002.06393 [hep-ex]].

21. A. M. Sirunyan *et al.* [CMS], "A measurement of the Higgs boson mass in the diphoton decay channel," Phys. Lett. B **805** (2020), 135425 doi:10.1016/j.physletb.2020.135425 [arXiv:2002.06398 [hep-ex]].

22. A. M. Sirunyan *et al.* [CMS], "Search for physics beyond the standard model in events with jets and two same-sign or at least three charged leptons in proton-proton collisions at $\sqrt{s}$ = 13 TeV," Eur. Phys. J. C **80** (2020) no.8, 752 doi:10.1140/epjc/s10052-020-8168-3 [arXiv:2001.10086 [hep-ex]].

23. A. M. Sirunyan *et al.* [CMS], "Search for charged Higgs bosons decaying into a top and a bottom quark in the all-jet final state of pp collisions at $\sqrt{s}$ = 13 TeV," JHEP **07** (2020), 126 doi:10.1007/JHEP07(2020)126 [arXiv:2001.07763 [hep-ex]].

24. A. M. Sirunyan *et al.* [CMS], "Measurement of the associated production of a $Z$ boson with charm or bottom quark jets in proton-proton collisions at $\sqrt{s}$=13 TeV," Phys. Rev. D **102** (2020) no.3, 032007 doi:10.1103/PhysRevD.102.032007 [arXiv:2001.06899 [hep-ex]].

25. A. M. Sirunyan *et al.* [CMS], "Study of excited $\Lambda_b^0$ states decaying to $\Lambda_b^0\pi^+\pi^-$ in proton-proton collisions at $\sqrt{s}$ = 13 TeV," Phys. Lett. B **803** (2020), 135345 doi:10.1016/j.physletb.2020.135345 [arXiv:2001.06533 [hep-ex]].